MobileDiffusion: Subsecond Text-to-Image Generation on Mobile Devices

Yang Zhao, Yanwu Xu, Zhisheng Xiao, Tingbo Hou

Google

{yzhaoeric, yanwuxu, zsxiao, tingbo}@google.com

(a) MobileDiffusion, distilled 8 steps

(b) MobileDiffusion, finetuned 1 step

Figure 1. MobileDiffusion text-to-image generation in (a) 8 steps (*cfg-aware* distillation [23]), and (b) 1 step (UFOGen finetuning [57]).

Abstract

*The deployment of large-scale text-to-image diffusion models on mobile devices is impeded by their substantial model size and slow inference speed. In this paper, we propose **MobileDiffusion**, a highly efficient text-to-image diffusion model obtained through extensive optimizations in both architecture and sampling techniques. We conduct a comprehensive examination of model architecture design to reduce redundancy, enhance computational efficiency, and minimize model's parameter count, while preserving image generation quality. Additionally, we employ distillation and diffusion-GAN finetuning techniques on MobileDiffusion to achieve 8-step and 1-step inference respectively. Empirical studies, conducted both quantitatively and qualitatively, demonstrate the effectiveness of our proposed techniques. MobileDiffusion achieves a remarkable **sub-second** inference speed for generating a 512×512 image on mobile devices, establishing a new state of the art.*

1. Introduction

Text-to-image diffusion models [1, 34, 36, 38, 39, 42] have exceptional capabilities in generating high-quality images conditioned on texts. These models serve as the foundation for a variety of applications, including image editing [12, 50], controlled generation [33, 60], personalized content generation [9, 41], video synthesis [3, 10], and low-level vision tasks [22, 55]. These large-scale models are essentially considered for necessarily running on servers with powerful neural compute units. Only a few work [20, 23] has barely touched designing diffusion models for mobile devices, which remains a open challenge.

The inefficiency of text-to-image diffusion models arises from two primary factors. Firstly, the inherent design of diffusion models requires iterative denoising to generate images, necessitating multiple evaluations of the model [14, 46]. Secondly, the complexity of the network architecture in text-to-image diffusion models involves a substantial number of parameters, often reaching into the billions, resulting in computationally expensive evaluations. These combined factors contribute to the high cost associated with deploying text-to-image diffusion models, limiting their practical utility in real-world scenarios. Moreover, the inefficiency challenge poses a significant barrier to the deployment of these models in resource-constrained environments, such as on mobile devices. As a result, despite the potential benefits of deploying generative models on mobile devices, such as enhancing user experience and

addressing emerging privacy concerns, this aspect remains relatively unexplored within the current literature.

The optimization of inference efficiency in text-to-image diffusion models has been a active research area. Previous studies predominantly concentrate on addressing the first factor, seeking to reduce the number of network evaluations. Leveraging advanced numerical solvers [2, 19, 28, 29, 45] or distillation techniques [23, 32, 43, 47], the necessary sampling steps have significantly reduced from several hundreds to around 10. Some recent techniques [25, 30, 57] even push the boundaries to a few or a single step. Despite these advancements, the deployment of diffusion models on edge devices is still a substantial challenge. On mobile devices, even a minimal number of evaluation steps can be slow or impractical, due to the second factor elucidated earlier — the computational intricacies associated with the model's architecture. Unfortunately, the architectural efficiency of text-to-image diffusion models has received comparatively less attention. A handful of earlier works briefly touch upon this matter, involving the removal of redundant neural network blocks [20, 23] or the reorganization of blocks [15] for enhanced efficiency. However, these efforts lack a comprehensive analysis of each component within the model architecture, thereby falling short of providing a holistic guide for designing highly efficient architectures.

Effectively overcoming the challenges imposed by limited computational power of on-device requires an in-depth and holistic exploration of the model's architectural efficiency. In pursuit of this objective, our research undertakes a detailed examination of each constituent and computational operation within the widely utilized UNet architecture [40]. Consequently, we present a comprehensive guide for crafting highly efficient text-to-image diffusion models. Drawing on these insights, our work introduces *MobileDiffusion*, embodying a delicately designed model architecture with fewer than 400 million parameters. This lightweight model emerges as a compelling choice for on-device applications, excelling not only in text-to-image generation but also in diverse downstream tasks. Furthermore, the resulting model seamlessly integrates with the techniques for reducing sampling steps discussed earlier. Notably, we successfully applied the sampling techniques [23, 57] to our model. The synergy of efficient architecture design and sampling step reduction empowers us to generate high-quality 512×512 images in **sub-second** on mobile devices, exemplified by **0.2 second** on iPhone 15 Pro. This remarkable result significantly surpasses the previous state-of-the-art in on-device text-to-image generation [23].

2. Related works

As elaborated in Section 1, to improve the inference efficiency of text-to-image diffusion models and ultimately enable their deployment on mobile devices, there are two primary areas of focus: *architecture efficiency* and *sampling efficiency*. We briefly review the prior work.

2.1. Architecture Efficiency

A limited number of prior works have discussed the architectural efficiency of diffusion models. [15] proposed the UViT architecture for training diffusion models on high-resolution images. They demonstrated that superior quality and efficiency could be achieved by scaling transformer blocks at the low-resolution segment of the UNet. [20] introduced an approach to distill larger diffusion models into smaller student models by selectively removing specific blocks from the teacher model. Meanwhile, [23] presented an efficient architecture search method. They trained a UNet with redundant blocks using robust training techniques [17, 58] and then pruned certain blocks based on metrics, resulting in an architecture suitable for distillation. In our work, we align with the insights of [15] regarding the transformer components in the UNet while introducing distinctive perspectives elaborated in Section 3. In contrast to approaches like [20, 23], our focus extends beyond mere block removal. Instead, we conduct a more nuanced analysis and modification of the architecture. Additionally, unlike [20, 23], we opt not to employ knowledge distillation from a larger model. Our observations indicate that training our model from scratch yields satisfactory results.

Our research is also closely related the broader domain of efficient architecture design, such as MobileNets [16], ConvNeXt [26], and Efficient Transformers [49].

2.2. Sample Efficiency

A fundamental challenge linked to diffusion models is the slow inference brought by the iterative denoising process. In response to this challenge, diverse strategies have emerged to expedite the required sampling speed, broadly falling into two categories. The first involves developing fast solvers to more efficiently solve the differential equation tied to the denoising process, thereby reducing the necessary discretization steps steps [2, 8, 19, 28, 28]. The second approach leverages knowledge distillation techniques to compress the sampling trajectory [23, 31, 43, 47]. Empirically, these techniques have demonstrated the ability to decrease the number of sampling steps to around 10 for latent diffusion models like Stable Diffusion (SD) [39]. However, further reductions often lead to a substantial drop in quality. Recent advancements, as presented in works like [25, 30, 57], introduce novel technologies pushing the boundaries of sampling step reduction to a few or even single steps.

3. Mobile Diffusion

In this section, we present our recipe for crafting highly efficient text-to-image diffusion models, which ultimately lead

to sub-second generation on mobile device. We start with a brief recap of Diffusion Models in Section 3.1. In section 3.2, we delve into a thorough investigation of UNet architecture optimization, with the goal of enhancing both parameter and runtime efficiency, while ensuring high-quality generation. In Section 3.3, we summarize the candidate architectures of Mobile Diffusion. Finally in Section 3.4, drawing inspiration from recent advancements in diffusion model distillation and diffusion GAN hybrids, we elucidate the methods we adopted for improving sample efficiency.

3.1. Preliminary: Diffusion Models

Diffusion models are trained to gradually transform a Gaussian noise to a sample from target data distribution $p(x)$ via a learned denoising process. After some derivation [14, 46], the training can be interpreted as a denoising process. Specifically, given a data point $x_0 \sim p(x)$, we can follow a schedule to add Gaussian noise ϵ to corrupt the clean data into a noisy version x_t, and the denoising network $\epsilon_\theta(x_t, t)$ is trained to predict the additive noise ϵ

$$\mathcal{L} = \mathbb{E}_{x,t,\epsilon \sim \mathcal{N}(0,\mathbf{I})} ||\epsilon - \epsilon_\theta(x_t, t)||_2^2. \quad (1)$$

Typically, the denoising network has a UNet structure [40], although alternative options exists [35]. For text-to-image generations, a text encoder $f(\cdot)$, usually frozen, transforms a prompt to a text embedding c. This embedding is subsequently input into the denoising network.

Text-to-image diffusion models can be broadly categorized to: pixel-based and latent-based models. Pixel-based models [1, 38, 42] directly model the pixel value, whereas latent-based models [36, 39] use a pre-trained Variational Autoencoder (VAE) to compress images into latent space, and let the diffusion models capture the distribution of latent variables. Latent diffusion models have demonstrated superiority in computational efficiency, making them a suitable candidate for low-cost applications such as on mobile devices. As a result, we primarily focus on the architecture design latent diffusion models, while the extension to pixel-based models is left for future exploration.

3.2. UNet Optimization

As illustrated in the left panel of Figure 2, UNet architectures for text-to-image diffusion models commonly interleave *transformer blocks* and *convolution blocks*. In this section, we conduct a comprehensive investigation of the these two fundamental building blocks. Throughout the study, we control the training pipeline (*e.g.* data, optimizer) to study the effects of different architectures. We leverage two metrics, Fréchet Inception Distance (FID) and CLIP-ViT B/32 on MS-COCO 2017 30K, complemented by visual inspections to measure the quality of each model variation. We start with a baseline model, which adopts the UNet architecture of SD [39]. After training with our pipeline, the

model obtains FID 12.45 and CLIP score 0.325 with the *cfg* weight set at 7.5, which is comparable with SD-1.5.

3.2.1 Transformer Blocks

In text-to-image diffusion models, a transformer block [51], as depicted in the right part of Figure 2, typically consists of a self-attention layer (SA) for modeling long-range dependencies among visual features, a cross-attention layer (CA) to capture interactions between text conditioning and visual features, and a feed-forward layer (FF) to post-process the output of attention layers. These transformer blocks hold a pivotal role in text-to-image diffusion models, serving as the primary components responsible for text comprehension. However, they also pose a significant efficiency challenge, given the computational expense of the attention operation. [15] introduced the UViT architecture, which places more transformer blocks at the bottleneck of the UNet. This design choice is motivated by that the attention computation is less resource-intensive at the bottleneck due to its lower dimensionality. At a high level, our architecture shares similarities with this approach. Nevertheless, we introduce several key modifications, elaborated below.

More transformers in the middle of Unet. Motivated by UViT[15], we adopt a strategic approach of relocating the parameters from high-resolution transformer blocks to lower resolutions while ensuring a consistent total parameter count. Maintaining this parameter count consistency can be achieved by reducing channel dimensions at lower resolutions. Our empirical observations indicate that this reduction does not adversely impact the quantitative metrics or the visual quality of the generated samples. Alternatively, to uphold the parameter count while accommodating more transformer blocks, one might consider reducing the width of the transformer. However, our investigations reveal that a substantial width of the transformer blocks is vital for optimal performance. Attempting to stack more transformer blocks with a smaller width proves detrimental, resulting in an evident degradation in visual quality characterized by poor object composition and intricate artifacts. These findings guide our design choice of incorporating more transformer blocks at lower resolutions while simultaneously reducing the number of channels at those resolutions.

With comparable model size, this modification improves run-time efficiency by 26% without quality drop.

Decouple SA from CA. In text-to-image diffusion models, self-attention plays a pivotal role in capturing long-range dependencies, although it comes with significant computational costs, especially at higher resolutions. For instance, at a resolution of 32×32, the sequence length for self-attention is 1024, resulting in an exceptionally high computational burden due to attention's quadratic complexity with
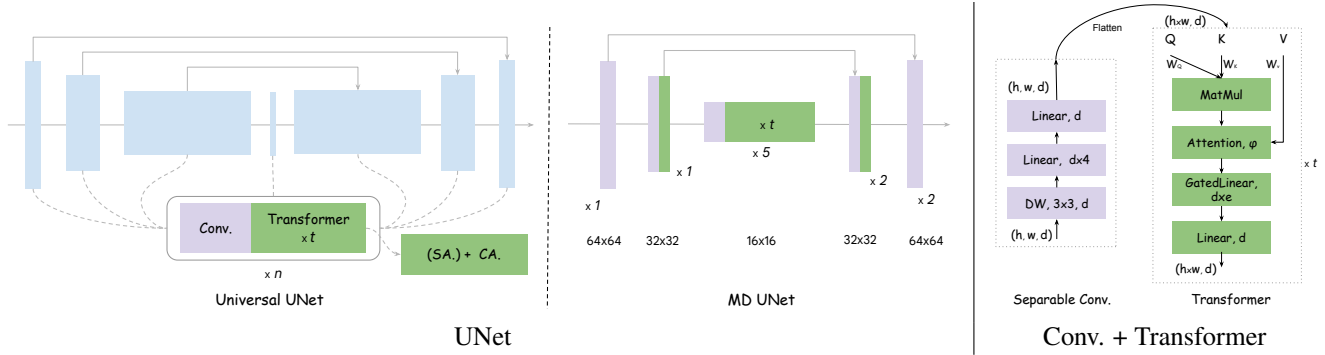
Figure 2. Model illustration of MobileDiffusion (MD). (Conv.: Convolution. SA: Self-attention (optional). CA: Cross-attention. ϕ: Non-linearity to calculate attention weights. e: Expansion factor in gated linear layer [44]. DW: Depth-wise convolution.)

respect to sequence length. In prior work, such as [15, 36], an approach involves relocating entire transformer blocks from high to lower resolutions, essentially removing both self-attention and cross-attention layers at high resolution. However, we observe that naively doing so leads to a notable performance decline. Specifically, the FID increases to 17.87 from the 12.50 baseline, and the CLIP score decreases to 0.302 from 0.325.

Upon further investigation, we discover that retaining cross-attention layers while discarding only the self-attention layers at high resolutions does not result in a performance drop. We conjecture that cross-attention is useful across different resolutions, as text guidance is crucial for both the global layout and local texture of the image. Notably, the computational cost of cross-attention at high resolution is significantly lower than that of self-attention, due to the smaller sequence length of text embeddings (*e.g.* 77 for SD). Consequently, removing only the self-attention layer yields a substantial efficiency boost. In light of these insights, we adopt a design that maintains performance while enhancing efficiency: entirely removing transformer blocks at the highest resolution (64×64); eliminating self-attention layers in the transformer blocks at 32×32 resolution and the outer 16×16 stack; retaining complete transformer blocks in the inner 16×16 stack and the innermost bottleneck stack.

This strategy improves computational efficiency by 15% without compromising model quality.

Share key-value projections. Within an attention layer, both the key and value are projected from the same input x, denoted as $K = x \cdot W_K$ and $V = x \cdot W_V$. Our experiments reveal that adopting a parameter-sharing scheme, specifically setting $W_K = W_V$ for self-attention layers, does not adversely affect model performance. Therefore, we choose to implement this parameter-sharing strategy, resulting in approximately a *5% reduction in parameter count.*

Replace gelu **with** swish. The GLU (Gated Linear Unit) [44] adopts the gelu activation function, a choice that unfortunately introduces numerical instability issues when employed in float16 or int8 inference on mobile devices due to the involvement of a cubic operation in the approximation [7]. Additionally, the gelu activation incurs slower computation, relying on specific hardware optimizations [48, 52]. Therefore, we propose substituting gelu with swish, which maintains a similar shape but is more cost-effective and computationally efficient. Importantly, empirical results indicate that this replacement does not lead to a degradation in metrics or perceptual quality.

This is optimized for post-training mobile deployment.

Finetune softmax **into** relu. Given key K, query Q and value V, attention calculates $\mathbf{x} = \phi(K^\mathsf{T}Q)V$, where the function $\phi(\cdot)$ is the softmax. However, the softmax function, where $\mathsf{softmax}(\mathbf{x}) = e^{\mathbf{x}} / \sum_{j=1}^{N} e^{x_j}$ and $\mathbf{x} = (x_0, x_1, ..., x_N)$, is computationally expensive due to non-efficient parallelization of exponentiation and summation across the sequence length. Conversely, point-wise activations like relu present a quicker alternative that does not rely on specific hardware optimizations, and it can serve as a viable substitute [53]. Consequently, we propose employing relu in our attention computation. An intriguing finding is that there is no need to train a relu-attention model from scratch; instead, finetuning from a pre-trained softmax-attention model proves sufficient, and this finetuning process can be accomplished quickly, for example, within 10,000 iterations. Visual ablation results for this modification are provided in Appendix. Interestingly, we even observe an improvement in FID compared to the relu-attention model, improved from 12.50 to 12.31.

This is also optimized across different mobile platforms.

Trim feed-forward layers. The initial UNet transformer block features a considerable expansion ratio of 8 in its feed-forward layers, leading to a dimensional surge from

1280 to 10240. However, such high dimensionality can be limiting in resource-constrained mobile applications. After thorough ablations, we found that trimming the expansion ratio to 6 results in nearly identical performance. With this adjustment, the FID score experiences only a slight increase from 12.31 to 12.58, while concurrently leading to *10% reduction in parameters count*.

3.2.2 Convolution Blocks

Convolution blocks, in particular ResNet blocks [11], are deployed at each level of the UNet. While these blocks are instrumental for feature extraction and information flow, the associated computational costs, especially at high-resolution levels, can be substantial. In this context, we delve into several critical insights aimed at enhancing the efficiency of convolution blocks.

Separable convolution. Residual blocks in vanilla convolutional layers typically involve a substantial number of parameters, prompting various endeavors to enhance the parameter efficiency of convolutional layers. One proven approach in this context is separable convolution [16]. We have observed that replacing vanilla convolution layers with lightweight separable convolution layers in the deeper segments of the UNet yields similar performance. As a result, we replace all the convolutional layers in the UNet with separable convolutionas, except for the outermost level. The separable convolutional block we adopted, as illustrated in Figure 2, shares similarities with ConvNeXt [26] but employs a smaller 3×3 kernel size. While we experimented with larger kernel sizes, such as 7×7 and 9×9, we found that they did not provide additional improvements.

This substitution enables us to reduce the model's parameter count by approximately 10%.

Prune redundant residual blocks. Convolution operations on high-resolution feature maps are especially computationally expensive, and pruning the convolution blocks is a straightforward way to improve model efficiency. Through comprehensive studies, we can effectively reduce the number of required residual blocks from the previous 22 (in SD) to a more efficient and streamlined 12. More specifically, we set 1 layer per block instead of 2 in SD, except for the innermost blocks. While maintaining a balance between resource consumption and model performance,

This pruning strategy optimizes computational efficiency by 19% and leads to 15% parameter reduction.

3.3. Architecture Candidates

Employing a the potential model architecture optimization techniques discussed earlier, we meticulously refine our selection of viable architecture candidates by imposing upper bounds on the number of parameters and floating-point operations per second (FLOPs). Specifically, for our model, denoted as MobileDiffusion (MD), we set a limit of 400 million parameters and 200 GFLOPs to ensure computational efficiency without compromising model performance. Notably, for ease of model search, we combine the innermost level of the down stack, the up stack, and the middle bottleneck into a unified module, as they share the same feature map dimension. This corresponds to the 5 layers in the middle of MD architecture as illustrated in Figure 2. Within this constrained search space, we systematically explore variations in the number of transformer layers and innermost channel dimensions, concentrating on the pivotal architectural parameters that significantly influence model performance. Due to the computational demands associated with training diffusion models, we prioritize optimizing these critical parameters to enhance the model's efficiency and effectiveness. In Table 1, we present a comparative analysis of our selected MD candidates, encompassing both the base model and a lightweight variant, against SD UNets and an on-device optimized SnapFusion UNet. The results underscore that our MD models exhibit a reduction in residual blocks, balanced attention layers, and enhanced parameter and runtime efficiency. Notably, the use of three blocks demonstrates superior visual attractiveness while maintaining comparable parameter counts, aligning with our earlier assertion that higher-level cross attention is integral to achieving high-quality diffusion models.

3.4. Sample Efficiency

In pursuit of sample efficiency, we employ off-the-self progressive distillation techniques [23, 32, 43]. The distillation method recursively condense the sampling trajectory of the teacher model into half number sampling steps. Our findings indicate that through distillation, a minimum of **8 steps** can be achieved without compromising image quality.

We additionally adopt the recent advances of diffusion-GAN hybrid models, such as [54, 56, 57]. In particular, we implement UFOGen [57] on our model. [57] proposes to finetune the pre-trained diffusion model with an hybrid objective of reconstruction term and adversarial term. This approach have demonstrated remarkable capabilities to transform a pre-trained diffusion model into a **single-step** generative model, pushing the sampling efficiency of diffusion models to a new level.

4. Experiments

We begin by providing an overview of the training specifics in Section 4.1, which encompass experimental setup, dataset, and the evaluation protocol. In Section 4.2, following that, we present the primary results of our text-to-image generation including both *cfg*-aware distilled and UFO finetuned models, including quantitative metrics, generated samples, perceptual assessments, as well as on-

Models	#Channels	#ConvBlocks	#(SA+CA)	#Params(M)	#GFLOPs	Latency(ms)	Model Size (GB)
SD-XL [36]	(320, 640, 1280)	17	31+31	2,300	710	29.5	5.66
SD-1.4/1.5	(320, 640, 1280, 1280)	22	16+16	862	392	21.7	2.07
SnapFusion [23]	(320, 640, 1280, 1280)	18	14+14	848	285	15.0	1.97
MobileDiffusion	(320, 640, 1024)	11	15+18	386	182	9.9	1.04
MobileDiffusion-Lite	(320, 640, 896)	11	12+15	278	153	8.8	0.82

Table 1. Comparison with other recognized latent diffusion models. Latency and GFLOPs, computed with jit per forward step, are measured for an input latent size of 64×64 on TPU v3. Model size (fp16) includes all, *i.e.*, UNet, text encoder and VAE decoder.

Decoders	#Params(M)	PSNR↑	SSIM↑	LPIPS↓	Latency(ms)
SD	49.5	26.7	0.76	0.037	200
Original	39.3	30.0	0.83	0.032	125
Ours	**9.8**	30.2	0.84	0.032	**65**

Table 2. Decoder variants before and after finetuning.

device benchmarks. Building upon the foundation of the pre-trained MobileDiffusion models, in Section 4.3, we delve into an exploration of various mobile applications, such as the integration of controls through plugins and of personalization capabilities via LoRA finetuning.

4.1. Training

UNet We offer two versions of UNet as outlined in Table 1. When compared to SD-1.5, MobileDiffusion achieves a compression rate of 46.4%. Additionally, MobileDiffusion-Lite, characterized by a narrower model width and shallower transformer blocks, achieves even higher compression, reaching 29.9%. Both variants also demonstrate significant advantages in terms of inference efficiency.

Figure 3. VAE reconstruction comparison among SD decoder, our original decoder and retrained efficient decoder.

VAE In our model, we use the VAE with some modifications over the SD's VAE. Same as SD's VAE, our VAE encoder downsamples the spatial resolution of the image by $8\times$. Our encoder encodes a 3-channel RGB image into an 8-channel latent variable, instead of the 4 channels used in SD. This modification enhances the quality of image reconstruction, as demonstrated in Figure 3. Similar to other VAEs used for latent diffusion models, our VAE is trained with a combination of loss functions, including $\mathcal{L}_2$ reconstruction loss, KL divergence for regularization, perceptual loss, and adversarial loss. We train the VAE with batch size 256 for 2 million iterations using the same dataset for diffusion model training.

To further enhance efficiency, we design a lightweight decoder architecture by pruning the original one's *width* and *depth*. We trained the lightweight decoder for 400K iterations with the encoder frozen. Since the encoder is frozen, we remove the unnecessary KL regularization in the objective. We also reduce the weight of adversarial loss. The resulting lightweight decoder leads to a significant performance boost, with nearly 50% latency improvement when decoding a 512×512 image. Quantitative comparison on COCO2017 validation in Table 2 shows the lightweight decoder's quality is on par with the original one.

Text Encoder We use OpenAI CLIP-ViT/L14 [37] as used in SD for text encoding, which is known to be powerful with a relatively compact size.

Dataset Our training process leverages a proprietary dataset, comprising an extensive collection of 150 million image-text pairs from public web [5]. The majority of images have a resolution greater than 256×256, and 40 million images with a resolution over 512×512. To prepare these images for training, we follow a consistent preprocessing methodology. Specifically, we crop the largest central square from each image and resize it to match the desired resolution.

Optimization Our models are trained with the AdamW optimizer [27], configured with a learning rate (lr) of 0.001, β_1 of 0.9, β_2 of 0.999, and a weight decay of 0.01. For image resolutions of 256×256, we employed a batch size of 4,096, while for resolutions of 512×512, the batch size was set at 2,048. The training process encompassed two phases: first, we trained at 256×256 resolution for 0.75M steps to capture high-level semantics, followed by an additional
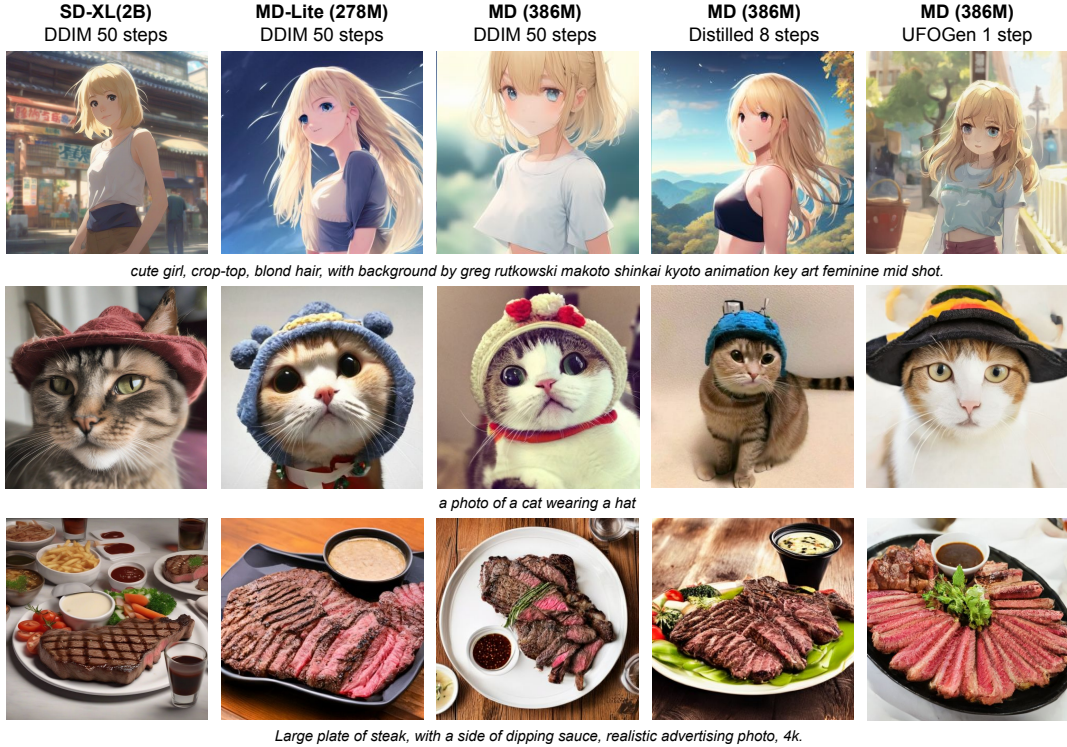
| SD-XL(2B) | MD-Lite (278M) | MD (386M) | MD (386M) | MD (386M) |
| DDIM 50 steps | DDIM 50 steps | DDIM 50 steps | Distilled 8 steps | UFOGen 1 step |

cute girl, crop-top, blond hair, with background by greg rutkowski makoto shinkai kyoto animation key art feminine mid shot.

a photo of a cat wearing a hat

Large plate of steak, with a side of dipping sauce, realistic advertising photo, 4k.

Table 3. Qualitative comparison between SD-XL, MD-Lite, and MD in DDIM 50 steps, as well as MD-distilled and MD-UFOGen.

0.25M steps at a resolution of 512×512 to refine features.

Training Cost When searching and selecting superior candidates, we have found that it suffices to rely on the FID and CLIP scores reported at the 30K iteration mark before which better designs can already produce text-image aligned results. This corresponds to approximately 4 hours of computation using 32 TPUs with 16GB memory each. We have designed a stopping mechanism for our experiments, which halts when the FID and CLIP scores show signs of slower improvement compared to previous candidates. This strategy works reasonable well in the process. In total, our endeavor consumes approximately 512 TPUs spanning 30 days to complete the refinement of MDs. The training duration for both MD and MD-Lite spans approximately 5 days in total.

Metrics We employed the MS-COCO dataset [24] as the primary source for our evaluations. In line with established practices, we present results for the zero-shot FID-30K scenario, where 30,000 captions are randomly selected from the COCO validation set. These captions serve as inputs for the image synthesis process. We calculate the FID score [13] to gauge the dissimilarity between the generated samples and the 30,000 reference ground truth images. Additionally, we provide the CLIP score [37], which assesses the average similarity between the generated sam-

ples and their corresponding input captions by utilizing features extracted from a pre-trained CLIP model, OpenCLIP-ViT/g14 [6].

4.2. Main Results

We present comprehensive results of the efficiency and quality of text to image generation, spanning quantitative and qualitative comparisons, and on-device benchmarks.

Quantitative Evaluation In Table 4, we conducted a comprehensive comparison of various text-to-image generative models. We prioritized sample efficiency by employing both *cfg-aware* distillation [23] and UFOGen [57] fine-tuning techniques, and we present the corresponding numerical results. For DDIM and the distilled models, we achieved the lowest FID scores by adjusting the *cfg* scales around 3.0. Since UFOGen does not involve *cfg*, we report the FID scores as is. We replicated the training settings of SD to match those of MD for a fair comparison. Our primary focus is on comparing our models using various samplers and the SD-replicated baseline, as FID evaluation can be subject to noise variations across different research works. The MD DDIM achieves a performance level close to that of the baseline SD-replicated model while being 50% smaller and 50% faster. Comparing the distilled 8-step model and the UFOGen finetuned 1-step model, we observe that their FID scores are comparable. Addition-

Models	Sample	#Steps	FID-30K↓	#Params(B)	#Data(B)
GigaGAN [18]	GAN	1	9.09	0.9	0.98
LAFITE [62]	GAN	1	26.94	0.23	0.003
Parti [59]	AR	-	7.23	20.0	5.00
DALL·E-2 [38]	DDPM	292	10.39	5.20	0.25
GLIDE [34]	DDPM	250	12.24	5.00	0.25
Imagen [42]	DDPM	256	7.27	3.60	0.45
SD [39]	DDIM	50	8.59	0.86	0.60
SnapFusion [23]	Distilled	8	13.5	0.85	-
PIXART-α [4]	DPM	20	10.65	0.6	0.025
BK-SDM [21]	DDIM	50	16.54	0.50	-
SD-replicated[1]	DDIM	50	8.43	0.86	0.15
MD	DDIM	50	8.65		
	Distilled	8	9.01	0.40	0.15
	UFOGen	1	11.67		
MD-Lite	DDIM	50	9.45		
	Distilled	8	9.87	0.26	0.15
	UFOGen	1	12.89		

Table 4. Quantitative evaluations on zero-shot MS-COCO.

ally, we compute the CLIP-ViT-g/14 score, and it's worth noting that both models can achieve around 0.33. This further highlights the effectiveness of our approach in achieving sample efficiency.

Qualitative Comparison In Table 3, we present a visual comparison between SD-XL, MD, distilled MD with 8 steps, and UFOGen finetuned with 1 step. Notably, MD consistently produces high-quality results across various types of samplers, even when compared to the strong baseline SD-XL. This demonstrates the potential for on-device applications. More examples can be found in Appendix.

On-device Benchmark We conducted benchmarking of our proposed MD using tools[2] on iPhone 15 Pro. As depicted in Table 5, MD exhibits superior efficiency in various aspects, including the text encoder, VAE decoder, UNet per-step inference, and the resulting overall latency, for both the distilled 8-step and finetuned 1-step models.

| Models	Text Encoder	Decoder	UNet	Steps	Overall
SnapFusion [23][3]	4	116	230	8	1960
UFOGen	4	285	1580	1	1869
MD	4	92	142	8	1232
				1	238
MD-Lite	4	92	123	1	219

Table 5. On-device latency (ms) measurements.

4.3. Applications

Our primary focus is on investigating on-device applications, particularly in the context of lightweight controllable adapters [33, 61] and LoRA fine-tuning. An essential challenge lies in determining whether distilled models or finetuned models are better suited for these applications. For both *cfg-aware* distilled and UFOGen finetuned models, we
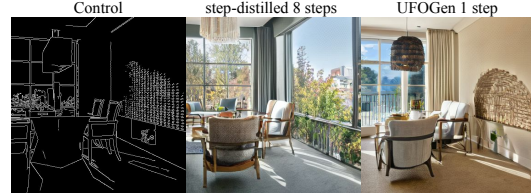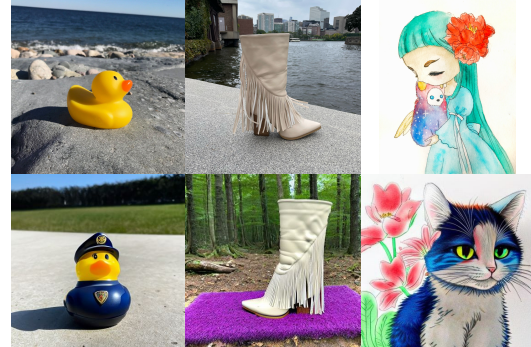

(a) Canny edge to image. *Prompt: a cozy living room*

(b) LoRA fine-tuning. Top row depicts the subject/style images and bottom row shows generated images.

Figure 4. Example applications of MobileDiffusion.

have explored methods for finetuning them in the realm of controllable text-to-image generation. In the case of translating canny edge to images, we were able to achieve comparable results by finetuning the adapters exclusively. However, for the more complex task of LoRA, we successfully accomplished our goal with the distilled model by finetuning only on the distilled timesteps. Figure 4 visually illustrates that MD can generate high-quality samples in the context of controllable text-to-image tasks.

5. Conclusions

In this paper, we explore pushing the boundary of diffusion model's efficiency by proposing MobileDiffusion, with the ultimate goal of democratizing text-to-image generation on mobile device. To achieve this goal, we conduct comprehensive studies of the architecture optimization for text-to-image diffusion models, which is a rarely touched area in prior work. Through the studies, we obtained a highly optimized architecture for diffusion UNet, with less than 400 million parameters and more efficient computational operations, while maintaining the quality. Additionally, we apply existing methods for reducing the sampling steps on MobileDiffusion, including progressive distillation and GAN finetuning. With the combined techniques, we are able to achieve the astonishing inference time of less than one second on mobile devices. We also showcase the versatility and utility of MobileDiffusion across a spectrum of text-to-image tasks, featuring its effectiveness for various downstream applications.

---

[1]We replicated SD on our training data and pipeline.

[2]https://github.com/apple/ml-stable-diffusion/tree/main.

[3]Numbers are from [23], measured on iPhone 14 Pro.

References

[1] Yogesh Balaji, Seungjun Nah, Xun Huang, Arash Vahdat, Jiaming Song, Karsten Kreis, Miika Aittala, Timo Aila, Samuli Laine, Bryan Catanzaro, et al. ediffi: Text-to-image diffusion models with an ensemble of expert denoisers. *arXiv preprint arXiv:2211.01324*, 2022. 1, 3

[2] Fan Bao, Chongxuan Li, Jun Zhu, and Bo Zhang. Analytic-dpm: an analytic estimate of the optimal reverse variance in diffusion probabilistic models. *arXiv preprint arXiv:2201.06503*, 2022. 2

[3] Andreas Blattmann, Robin Rombach, Huan Ling, Tim Dockhorn, Seung Wook Kim, Sanja Fidler, and Karsten Kreis. Align your latents: High-resolution video synthesis with latent diffusion models. In *Proceedings of the IEEE/CVF Conference on Computer Vision and Pattern Recognition*, pages 22563–22575, 2023. 1

[4] Junsong Chen, Jincheng Yu, Chongjian Ge, Lewei Yao, Enze Xie, Yue Wu, Zhongdao Wang, James Kwok, Ping Luo, Huchuan Lu, et al. Pixart-α: Fast training of diffusion transformer for photorealistic text-to-image synthesis. *arXiv preprint arXiv:2310.00426*, 2023. 8

[5] Xi Chen, Xiao Wang, Soravit Changpinyo, AJ Piergiovanni, Piotr Padlewski, Daniel Salz, Sebastian Goodman, Adam Grycner, Basil Mustafa, Lucas Beyer, Alexander Kolesnikov, Joan Puigcerver, Nan Ding, Keran Rong, Hassan Akbari, Gaurav Mishra, Linting Xue, Ashish Thapliyal, James Bradbury, Weicheng Kuo, Mojtaba Seyedhosseini, Chao Jia, Burcu Karagol Ayan, Carlos Riquelme, Andreas Steiner, Anelia Angelova, Xiaohua Zhai, Neil Houlsby, and Radu Soricut. Pali: A jointly-scaled multilingual language-image model. In *International Conference on Learning Representations*, 2023. 6

[6] Mehdi Cherti, Romain Beaumont, Ross Wightman, Mitchell Wortsman, Gabriel Ilharco, Cade Gordon, Christoph Schuhmann, Ludwig Schmidt, and Jenia Jitsev. Reproducible scaling laws for contrastive language-image learning. In *Proceedings of the IEEE/CVF Conference on Computer Vision and Pattern Recognition*, pages 2818–2829, 2023. 7

[7] Jiwoong Choi, Minkyu Kim, Daehyun Ahn, Taesu Kim, Yulhwa Kim, Dongwon Jo, Hyesung Jeon, Jae-Joon Kim, and Hyungjun Kim. Squeezing large-scale diffusion models for mobile. *arXiv preprint arXiv:2307.01193*, 2023. 4

[8] Tim Dockhorn, Arash Vahdat, and Karsten Kreis. Genie: Higher-order denoising diffusion solvers. *Advances in Neural Information Processing Systems*, 35:30150–30166, 2022. 2

[9] Rinon Gal, Yuval Alaluf, Yuval Atzmon, Or Patashnik, Amit Haim Bermano, Gal Chechik, and Daniel Cohen-or. An image is worth one word: Personalizing text-to-image generation using textual inversion. In *The Eleventh International Conference on Learning Representations*, 2022. 1

[10] Yuwei Guo, Ceyuan Yang, Anyi Rao, Yaohui Wang, Yu Qiao, Dahua Lin, and Bo Dai. Animatediff: Animate your personalized text-to-image diffusion models without specific tuning. *arXiv preprint arXiv:2307.04725*, 2023. 1

[11] Kaiming He, Xiangyu Zhang, Shaoqing Ren, and Jian Sun. Deep residual learning for image recognition. In *Proceedings of the IEEE conference on computer vision and pattern recognition*, pages 770–778, 2016. 5

[12] Amir Hertz, Ron Mokady, Jay Tenenbaum, Kfir Aberman, Yael Pritch, and Daniel Cohen-Or. Prompt-to-prompt image editing with cross attention control. *arXiv preprint arXiv:2208.01626*, 2022. 1

[13] Martin Heusel, Hubert Ramsauer, Thomas Unterthiner, Bernhard Nessler, and Sepp Hochreiter. Gans trained by a two time-scale update rule converge to a local nash equilibrium. *Advances in neural information processing systems*, 30, 2017. 7

[14] Jonathan Ho, Ajay Jain, and Pieter Abbeel. Denoising diffusion probabilistic models. *Advances in neural information processing systems*, 33:6840–6851, 2020. 1, 3

[15] Emiel Hoogeboom, Jonathan Heek, and Tim Salimans. simple diffusion: End-to-end diffusion for high resolution images. *arXiv preprint arXiv:2301.11093*, 2023. 2, 3, 4

[16] Andrew G Howard, Menglong Zhu, Bo Chen, Dmitry Kalenichenko, Weijun Wang, Tobias Weyand, Marco Andreetto, and Hartwig Adam. Mobilenets: Efficient convolutional neural networks for mobile vision applications. *arXiv preprint arXiv:1704.04861*, 2017. 2, 5

[17] Gao Huang, Yu Sun, Zhuang Liu, Daniel Sedra, and Kilian Q Weinberger. Deep networks with stochastic depth. In *Computer Vision–ECCV 2016: 14th European Conference, Amsterdam, The Netherlands, October 11–14, 2016, Proceedings, Part IV 14*, pages 646–661. Springer, 2016. 2

[18] Minguk Kang, Jun-Yan Zhu, Richard Zhang, Jaesik Park, Eli Shechtman, Sylvain Paris, and Taesung Park. Scaling up gans for text-to-image synthesis. In *Proceedings of the IEEE/CVF Conference on Computer Vision and Pattern Recognition*, pages 10124–10134, 2023. 8

[19] Tero Karras, Miika Aittala, Timo Aila, and Samuli Laine. Elucidating the design space of diffusion-based generative models. *Advances in Neural Information Processing Systems*, 35:26565–26577, 2022. 2

[20] Bo-Kyeong Kim, Hyoung-Kyu Song, Thibault Castells, and Shinkook Choi. On architectural compression of text-to-image diffusion models. *arXiv preprint arXiv:2305.15798*, 2023. 1, 2

[21] Bo-Kyeong Kim, Hyoung-Kyu Song, Thibault Castells, and Shinkook Choi. BK-SDM: Architecturally compressed stable diffusion for efficient text-to-image generation. In *Workshop on Efficient Systems for Foundation Models @ ICML2023*, 2023. 8

[22] Alexander C Li, Mihir Prabhudesai, Shivam Duggal, Ellis Brown, and Deepak Pathak. Your diffusion model is secretly a zero-shot classifier. *arXiv preprint arXiv:2303.16203*, 2023. 1

[23] Yanyu Li, Huan Wang, Qing Jin, Ju Hu, Pavlo Chemerys, Yun Fu, Yanzhi Wang, Sergey Tulyakov, and Jian Ren. Snapfusion: Text-to-image diffusion model on mobile devices within two seconds. *arXiv preprint arXiv:2306.00980*, 2023. 1, 2, 5, 6, 7, 8

[24] Tsung-Yi Lin, Michael Maire, Serge Belongie, James Hays, Pietro Perona, Deva Ramanan, Piotr Dollár, and C Lawrence Zitnick. Microsoft coco: Common objects in context. In

Computer Vision–ECCV 2014: 13th European Conference, Zurich, Switzerland, September 6-12, 2014, Proceedings, Part V 13, pages 740–755. Springer, 2014. 7

[25] Xingchao Liu, Xiwen Zhang, Jianzhu Ma, Jian Peng, and Qiang Liu. Instaflow: One step is enough for high-quality diffusion-based text-to-image generation. *arXiv preprint arXiv:2309.06380*, 2023. 2

[26] Zhuang Liu, Hanzi Mao, Chao-Yuan Wu, Christoph Feichtenhofer, Trevor Darrell, and Saining Xie. A convnet for the 2020s. In *Proceedings of the IEEE/CVF conference on computer vision and pattern recognition*, pages 11976–11986, 2022. 2, 5

[27] Ilya Loshchilov and Frank Hutter. Decoupled weight decay regularization. In *International Conference on Learning Representations*, 2018. 6

[28] Cheng Lu, Yuhao Zhou, Fan Bao, Jianfei Chen, Chongxuan Li, and Jun Zhu. Dpm-solver: A fast ode solver for diffusion probabilistic model sampling in around 10 steps. *Advances in Neural Information Processing Systems*, 35:5775–5787, 2022. 2

[29] Cheng Lu, Yuhao Zhou, Fan Bao, Jianfei Chen, Chongxuan Li, and Jun Zhu. Dpm-solver++: Fast solver for guided sampling of diffusion probabilistic models. *arXiv preprint arXiv:2211.01095*, 2022. 2

[30] Simian Luo, Yiqin Tan, Longbo Huang, Jian Li, and Hang Zhao. Latent consistency models: Synthesizing high-resolution images with few-step inference. *arXiv preprint arXiv:2310.04378*, 2023. 2

[31] Chenlin Meng, Yutong He, Yang Song, Jiaming Song, Jiajun Wu, Jun-Yan Zhu, and Stefano Ermon. Sdedit: Guided image synthesis and editing with stochastic differential equations. In *International Conference on Learning Representations*, 2021. 2

[32] Chenlin Meng, Robin Rombach, Ruiqi Gao, Diederik Kingma, Stefano Ermon, Jonathan Ho, and Tim Salimans. On distillation of guided diffusion models. In *Proceedings of the IEEE/CVF Conference on Computer Vision and Pattern Recognition*, pages 14297–14306, 2023. 2, 5

[33] Chong Mou, Xintao Wang, Liangbin Xie, Jian Zhang, Zhongang Qi, Ying Shan, and Xiaohu Qie. T2i-adapter: Learning adapters to dig out more controllable ability for text-to-image diffusion models. *arXiv preprint arXiv:2302.08453*, 2023. 1, 8

[34] Alexander Quinn Nichol, Prafulla Dhariwal, Aditya Ramesh, Pranav Shyam, Pamela Mishkin, Bob Mcgrew, Ilya Sutskever, and Mark Chen. Glide: Towards photorealistic image generation and editing with text-guided diffusion models. In *International Conference on Machine Learning*, pages 16784–16804. PMLR, 2022. 1, 8

[35] William Peebles and Saining Xie. Scalable diffusion models with transformers. In *Proceedings of the IEEE/CVF International Conference on Computer Vision*, pages 4195–4205, 2023. 3

[36] Dustin Podell, Zion English, Kyle Lacey, Andreas Blattmann, Tim Dockhorn, Jonas Müller, Joe Penna, and Robin Rombach. Sdxl: improving latent diffusion models for high-resolution image synthesis. *arXiv preprint arXiv:2307.01952*, 2023. 1, 3, 4, 6

[37] Alec Radford, Jong Wook Kim, Chris Hallacy, Aditya Ramesh, Gabriel Goh, Sandhini Agarwal, Girish Sastry, Amanda Askell, Pamela Mishkin, Jack Clark, et al. Learning transferable visual models from natural language supervision. In *International conference on machine learning*, pages 8748–8763. PMLR, 2021. 6, 7

[38] Aditya Ramesh, Prafulla Dhariwal, Alex Nichol, Casey Chu, and Mark Chen. Hierarchical text-conditional image generation with clip latents. *arXiv preprint arXiv:2204.06125*, 1 (2):3, 2022. 1, 3, 8

[39] Robin Rombach, Andreas Blattmann, Dominik Lorenz, Patrick Esser, and Björn Ommer. High-resolution image synthesis with latent diffusion models. In *Proceedings of the IEEE/CVF conference on computer vision and pattern recognition*, pages 10684–10695, 2022. 1, 2, 3, 8

[40] Olaf Ronneberger, Philipp Fischer, and Thomas Brox. U-net: Convolutional networks for biomedical image segmentation. In *Medical Image Computing and Computer-Assisted Intervention–MICCAI 2015: 18th International Conference, Munich, Germany, October 5-9, 2015, Proceedings, Part III 18*, pages 234–241. Springer, 2015. 2, 3

[41] Nataniel Ruiz, Yuanzhen Li, Varun Jampani, Yael Pritch, Michael Rubinstein, and Kfir Aberman. Dreambooth: Fine tuning text-to-image diffusion models for subject-driven generation. In *Proceedings of the IEEE/CVF Conference on Computer Vision and Pattern Recognition*, pages 22500–22510, 2023. 1

[42] Chitwan Saharia, William Chan, Saurabh Saxena, Lala Li, Jay Whang, Emily L Denton, Kamyar Ghasemipour, Raphael Gontijo Lopes, Burcu Karagol Ayan, Tim Salimans, et al. Photorealistic text-to-image diffusion models with deep language understanding. *Advances in Neural Information Processing Systems*, 35:36479–36494, 2022. 1, 3, 8

[43] Tim Salimans and Jonathan Ho. Progressive distillation for fast sampling of diffusion models. In *International Conference on Learning Representations*, 2022. 2, 5

[44] Noam Shazeer. Glu variants improve transformer. *arXiv preprint arXiv:2002.05202*, 2020. 4

[45] Jiaming Song, Chenlin Meng, and Stefano Ermon. Denoising diffusion implicit models. In *International Conference on Learning Representations*, 2020. 2

[46] Yang Song, Jascha Sohl-Dickstein, Diederik P Kingma, Abhishek Kumar, Stefano Ermon, and Ben Poole. Score-based generative modeling through stochastic differential equations. In *International Conference on Learning Representations*, 2020. 1, 3

[47] Yang Song, Prafulla Dhariwal, Mark Chen, and Ilya Sutskever. Consistency models. 2023. 2

[48] Zhiqing Sun, Hongkun Yu, Xiaodan Song, Renjie Liu, Yiming Yang, and Denny Zhou. Mobilebert: a compact task-agnostic bert for resource-limited devices. In *Proceedings of the 58th Annual Meeting of the Association for Computational Linguistics*, pages 2158–2170, 2020. 4

[49] Yi Tay, Mostafa Dehghani, Dara Bahri, and Donald Metzler. Efficient transformers: A survey. *ACM Comput. Surv.*, 55(6), 2022. 2

[50] Narek Tumanyan, Michal Geyer, Shai Bagon, and Tali Dekel. Plug-and-play diffusion features for text-driven

image-to-image translation. In *Proceedings of the IEEE/CVF Conference on Computer Vision and Pattern Recognition*, pages 1921–1930, 2023. 1

[51] Ashish Vaswani, Noam Shazeer, Niki Parmar, Jakob Uszkoreit, Llion Jones, Aidan N Gomez, Łukasz Kaiser, and Illia Polosukhin. Attention is all you need. *Advances in neural information processing systems*, 30, 2017. 3

[52] Xudong Wang, Li Lyna Zhang, Yang Wang, and Mao Yang. Towards efficient vision transformer inference: A first study of transformers on mobile devices. In *Proceedings of the 23rd Annual International Workshop on Mobile Computing Systems and Applications*, pages 1–7, 2022. 4

[53] Mitchell Wortsman, Jaehoon Lee, Justin Gilmer, and Simon Kornblith. Replacing softmax with relu in vision transformers. *arXiv preprint arXiv:2309.08586*, 2023. 4

[54] Zhisheng Xiao, Karsten Kreis, and Arash Vahdat. Tackling the generative learning trilemma with denoising diffusion gans. In *International Conference on Learning Representations*, 2022. 5

[55] Jiarui Xu, Sifei Liu, Arash Vahdat, Wonmin Byeon, Xiaolong Wang, and Shalini De Mello. Open-vocabulary panoptic segmentation with text-to-image diffusion models. In *Proceedings of the IEEE/CVF Conference on Computer Vision and Pattern Recognition*, pages 2955–2966, 2023. 1

[56] Yanwu Xu, Mingming Gong, Shaoan Xie, Wei Wei, Matthias Grundmann, Tingbo Hou, et al. Semi-implicit denoising diffusion models (siddms). *arXiv preprint arXiv:2306.12511*, 2023. 5

[57] Yanwu Xu, Yang Zhao, Zhisheng Xiao, and Tingbo Hou. Ufogen: You forward once large scale text-to-image generation via diffusion gans. *arXiv preprint arXiv:2311.09257*, 2023. 1, 2, 5, 7

[58] Jiahui Yu, Linjie Yang, Ning Xu, Jianchao Yang, and Thomas Huang. Slimmable neural networks. In *International Conference on Learning Representations*, 2018. 2

[59] Jiahui Yu, Yuanzhong Xu, Jing Yu Koh, Thang Luong, Gunjan Baid, Zirui Wang, Vijay Vasudevan, Alexander Ku, Yinfei Yang, Burcu Karagol Ayan, et al. Scaling autoregressive models for content-rich text-to-image generation. *arXiv preprint arXiv:2206.10789*, 2(3):5, 2022. 8

[60] Lvmin Zhang, Anyi Rao, and Maneesh Agrawala. Adding conditional control to text-to-image diffusion models. In *Proceedings of the IEEE/CVF International Conference on Computer Vision*, pages 3836–3847, 2023. 1

[61] Yang Zhao and Tingbo Hou. On-device diffusion plugins for conditioned text-to-image generation. https://blog.research.google/2023/06/on-device-diffusion-plugins-for.html, 2023. 8

[62] Yufan Zhou, Ruiyi Zhang, Changyou Chen, Chunyuan Li, Chris Tensmeyer, Tong Yu, Jiuxiang Gu, Jinhui Xu, and Tong Sun. Towards language-free training for text-to-image generation. In *Proceedings of the IEEE/CVF Conference on Computer Vision and Pattern Recognition (CVPR)*, pages 17907–17917, 2022. 8

MobileDiffusion: Subsecond Text-to-Image Generation on Mobile Devices

Supplementary Material

6. Architecture Optimization

Here, we provide additional complementary details that were not covered in the primary section on architecture optimization. These details are intended to offer a more comprehensive understanding of the importance and necessity of certain components.

Replace gelu **with** swish. As observed in Eq. 2, the function gelu contains a cubic term that may lead to error accumulation or overflow concerns, particularly when implementing quantization. In contrast, swish as shown in Eq. 3 is computationally simpler, offering a solution to mitigate potential problems.

$$\text{gelu}(x) = x \cdot \Phi(x)$$
$$\approx 0.5x(1 + \tanh(\sqrt{\frac{2}{\pi}}(x + 0.044715x^3))) \quad (2)$$

where $\Phi(\cdot)$ is the cumulative distribution function for Gaussian distribution.

$$\text{swish}(x) = x \cdot \text{sigmoid}(x) \quad (3)$$

Finetune softmax **into** relu. Figure 5 presents a comparison of results obtained from models trained using the two activation functions. In our observations, there is rarely any noticeable visual distinction when using either of these activations in attention computations. However, employing the relu activation can significantly enhance mobile efficiency. As far as our knowledge extends, this represents the inaugural effort to effectively fine-tune a generative model initially activated with softmax into its relu counterpart.

A corgi's head depicted as an explosion of a nebula.

Figure 5. Visual comparison between using softmax (left) and relu (right).

7. Mobile Diffusion Architectures

In the main part, we have explained how we build efficient MD models step by step. Here we will show the detailed architectures of both MD and MD-lite in Table 6.

Models	Blocks	Layers	
		Conv	Transformer
MD	Down-1	FullConv ×1	-
	Down-2	FullConv ×1	CA
	Down-3	SPConv ×2	(SA ×3 + CA ×3)×2
	Up-3	SPConv ×3	(SA ×3 + CA ×3) ×3
	Up-2	FullConv ×2	CA ×2
	Up-1	FullConv ×2	-
MD-Lite	Down-1	FullConv ×1	-
	Down-2	FullConv ×1	CA
	Down-3	SPConv ×2	(SA ×3 + CA ×3) ×2
	Up-3	SPConv ×3	(SA ×2 + CA ×2) ×3
	Up-2	FullConv ×2	CA ×2
	Up-1	FullConv ×2	-

Table 6. Arcitecture details of MD and MD-Lite. FullConv means original residual blocks while SPConv uses Figure 2. A notable difference between MD and MD-Lite is innermost channels which are 1024 and 896 respectively.
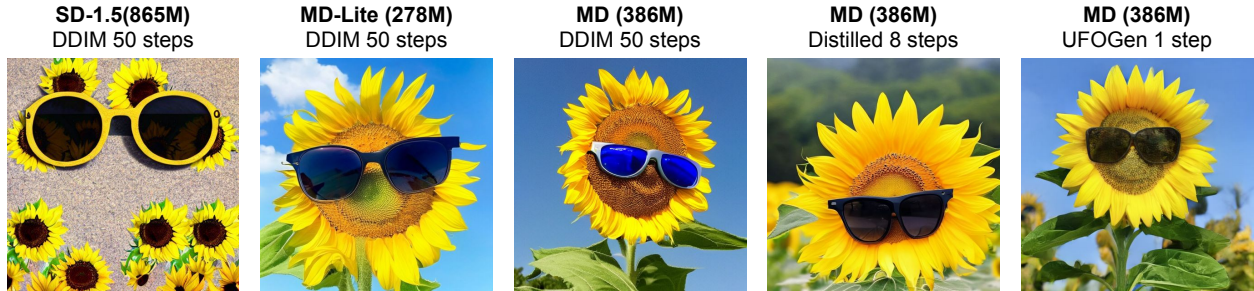
8. Extended Generated Examples

8.1. Qualitative Examples

In Figure 6, we present an extended comparison between SD-1.5 and our learned MD variants. We have chosen to use SD-1.5 for this comparison since it employs the same text encoder, OpenAI CLIP ViT/L14, as our models. Additionally, we have expanded our selection of prompts to encompass various topics, including style, imagination, and complex compositions, beyond what was originally covered in the main section. This extended comparison underscores the consistent ability of MD to generate visually appealing results and its superiority over SD-1.5 in correctly interpreting specific prompts, such as those related to color and relationship. In Figure 7, we show more photo-realistic generated samples from our 1-step MD model finetuned with UFOGen. In Figure 8, we generate more examples using same prompts as in Figure 7 from our distilled 8-step MD. Beyond applications of canny edge and LoRA control as mentioned in the main context, we also explored more difficult tasks, layout control and layout + LoRA control. We show qualitative results in Figure 9.

8.2. Failures Cases

In Figure 10, we illustrate two prevalent types of failures: uncommon knowledge and quantity interpretation. We at-

| **SD-1.5(865M)** | **MD-Lite (278M)** | **MD (386M)** | **MD (386M)** | **MD (386M)** |
| DDIM 50 steps | DDIM 50 steps | DDIM 50 steps | Distilled 8 steps | UFOGen 1 step |

A sunflower wearing sunglasses

A robot painted as graffiti on a brick wall. a sidewalk is in front of the wall, and grass is growing out of cracks in the concrete.

Watercolor painting of a corgi's head outline, where the inside is painted as a mesmerizing nebula with shades of purples, blues, and golds, amidst a vast cosmic backdrop.

A serious capybara wearing a suit.
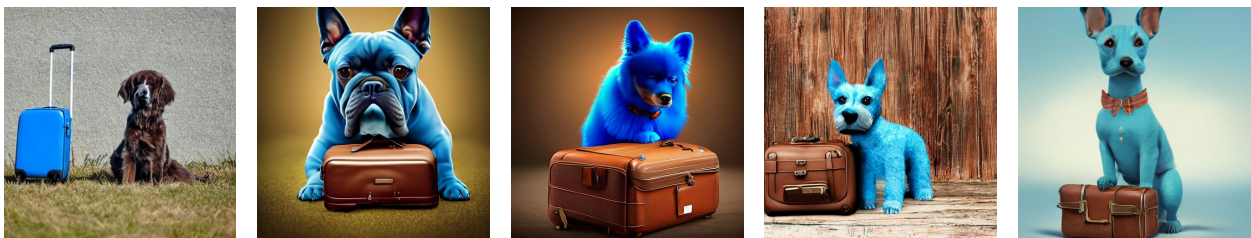
a blue dog and a brown suitcase, photo realistic

Figure 6. Extended qualitative comparison among SD-1.5 and a range of MD variants.

tribute these failures to the limited capabilities of the text encoder, as we have observed similar phenomena in both SD-1.5 and SD-XL.

Animals

People

Outdoor Scenes

Other Illustrations

Figure 7. Extended photo-realistic samples from finetuned 1-step MD.

Animals

People

Outdoor Scenes

Other Illustrations

Figure 8. Extended photo-realistic samples from distilled 8-step MD.

(a) Layout control. **Prompt**: *An astronaut riding a <u>horse</u>, highly realistic dslr photo, cinematic shot.*

Style

(b) Layout + LoRA Style control. **Prompt**: *a photo of <u>horse</u> in the forest.*

Figure 9. Extended applications of MD on layout control and the combination of layout and LoRA style control.

(a) *square blue apples on a tree with circular yellow leaves*

(b) *ten red apples*

Figure 10. Failure cases of MD.